Thin Solid Films 519 (2011) 5114–5117

Contents lists available at ScienceDirect

Thin Solid Films

journal homepage: www.elsevier.com/locate/tsf

Transparent conductive indium-doped zinc oxide films prepared by atmospheric pressure plasma jet

Kow-Ming Chang [a,b], Sung-Hung Huang [a,*], Chin-Jyi Wu [c], Wei-Li Lin [a], Wei-Chiang Chen [a], Chia-Wei Chi [a], Je-Wei Lin [c], Chia-Chiang Chang [c]

[a] Department of Electronics Engineering & Institute of Electronics, National Chiao Tung University, 1001 Ta Hsueh Road, Hsinchu, Taiwan 30010, ROC
[b] College of Electrical and Information Engineering, I-Shou University, Kaohsiung County, Taiwan 84001, ROC
[c] Industrial Technology Research Institute, Mechanical and Systems Research Laboratories, 195, Sec. 4, Chung Hsing Rd., Chutung, Hsinchu, 31040, Taiwan, ROC

ARTICLE INFO

Available online 20 January 2011

Keywords:
Transparent conductive oxide
Atmospheric-pressure plasma
Indium-doped zinc oxide
Zinc nitrate
Indium nitrate

ABSTRACT

Atmospheric-pressure plasma processing has attracted much interest for industrial applications due to its low cost, high processing speed and simple system. In this study, atmospheric-pressure plasma jet technique was developed to deposit indium-doped zinc oxide films. The inorganic metal salts of zinc nitrate and indium nitrate were used as precursors for Zn ions and In ions, respectively. The effect of different indium doping concentration on the morphological, structural, electrical and optical properties of the films was investigated. Grazing incidence X-ray diffraction results show that the deposited films with a preferred (002) orientation. The lowest resistivity of 1.8×10^{-3} Ω cm was achieved with the 8 at.% indium-doped solution at the substrate temperature of 200 °C in open air, and average transmittance in the visible region was more than 80%.

1. Introduction

Atmospheric pressure plasma is used in a variety of material processes, such as SiO_2 [1], TiO_2 [2], and ZnO thin films [3]. ZnO thin films have attracted much attention as the transparent conductive oxide due to their nontoxicity, low cost, and good stability in the hydrogen-containing plasma, which exists in the fabrication process of some optoelectronic devices. Un-doped ZnO thin films have n type properties due to intrinsic defects, but un-doped ZnO films have poor thermal stability. In order to increase the conductivity and stability of ZnO films, group-III elements (Al, Ga, and In) can be used as substitutional dopants for Zn site. Because indium has less reactivity and greater resistivity to oxidation than aluminum, indium has easier process controllability. ZnO-based thin films can be prepared on several substrates in a number of ways: pulse laser deposition [4,5], ion plating [6], RF magnetic sputtering [7], and metalorganic chemical vapor deposition [8]. Among the different techniques used for the growth of these layers, atmospheric pressure plasma jet (APPJ) has many advantages, such as its low cost and good suitability for large-scale applications, since it does not need a vacuum chamber and associated pumping system. Zinc oxide thin films have been reported by using atmospheric pressure plasma technique [9,10]. However, to our knowledge, no complete investigation was reported for indium-doped ZnO thin films deposited by APPJ. In this study, we develop indium-doped ZnO by using APPJ and discuss the effect of different indium doping concentration on the morphological, structural, electrical and optical properties of the films.

2. Experiment

Indium doped zinc oxide thin films were grown on glass substrates (2.5 cm × 2.5 cm × 0.7 cm) by APPJ. Fig. 1 shows a schematic diagram of the experimental apparatus for APPJ. The deposition apparatus mainly is composed of a plasma jet, an ultrasonic generator, and a hot plate. The DC pulse power supply and main gas generate the downstream plasma. For deposition of indium-doped ZnO films, the zinc nitrate ($Zn(NO_3)_2$,99% purity) and indium nitrate ($In(NO_3)_2$, 99.99% purity) were used as the precursor without further purification. Pure deionized water was used as a solvent and the concentration of zinc nitrate in the deionized water was kept at 0.2 M. The precursor, mixed different zinc nitrate with indium nitrate dissolved in deionized water, was prepared for different doping concentrations (In/Zn + In atomic ratios). Next, the solution was ultrasonically atomized at 2.45 MHz into mist and then conveyed by carrier gas to the plasma region. The nitrogen (N_2) was used as carrier gas and main gas. The flow rate of carrier gas was fixed at 300 sccm, while the flow rate of main gas was 35 SLM. The nozzle to substrate distance was 5 mm. The power was set at 600 W and substrate temperature was 200 °C, individually. In order to deposit uniform indium-doped ZnO thin film, the xy directional scan system was used. The position of plasma jet was fixed and the substrate was on the xy directional scan system. First, start point, endpoint and the pitch were set. Next, the scan system moved from the start point to the end point, and the scan was repeated 10 times. The pitch controlled the overlap of the two

* Corresponding author.
E-mail address: sunghunghuang@gmail.com (S.H. Huang).

0040-6090/$ – see front matter © 2011 Elsevier B.V. All rights reserved.
doi:10.1016/j.tsf.2011.01.156

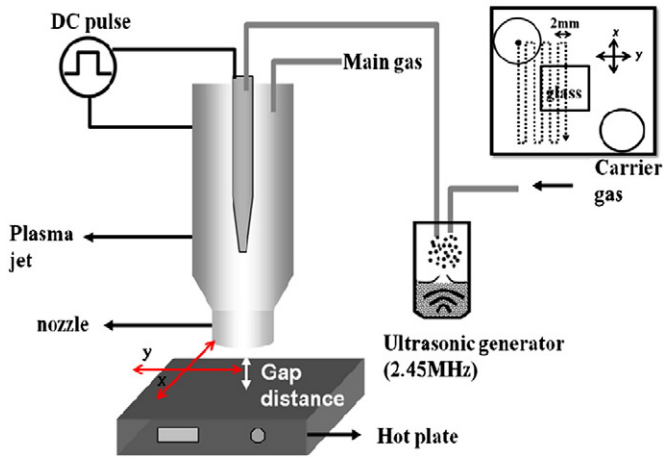

Fig. 1. Schematic diagram of the experimental apparatus.

paths of x direction. The scan path was shown in the inserted graph of Fig. 1. The scan rate of x direction was 20 mm/s, and the scan rate of y direction was 50 mm/s. The pitch was set at 2 mm.

The morphological, structural, electrical and optical properties of the indium-doped ZnO films were characterized in this work. The crystallinity of the indium-doped ZnO thin films was investigated by using grazing incidence X-ray diffraction (GIXRD), and the thickness as well as the morphological property was determined by scanning electron microscopy (SEM), respectively. The roughness was determined by atomic force microscopy (AFM). Electrical properties were measured by using Hall measurement. Optical transmission through the films on the glass was measured in the wavelength range from 300 nm to 800 nm by using a UV–VIS-NIR spectrophotometer.

3. Result and discussion

SEM images of different indium doping concentrations and RMS roughness of AFM from 0 at.% to 10 at.% were shown in Fig. 2. When the doping concentration becomes higher, the surface shows obviously needlelike geometry. As a result, the high indium content shows a rougher surface. D.H. Kim et al. proposed that the IZO thin films deposited by RF magnetron sputter show the needlelike geometry. It is thought that the indium lies distributed randomly on the ZnO film, thus preventing an orderly arrangement [7]. Fig. 3 presents the GIXRD patterns of different indium-doped ZnO films deposited by APPJ at the substrate temperature of 200 °C. Indium-doped ZnO films demonstrate a high (002) preferential orientation, meaning that the c-axis of the crystal lattice is normal to the plane of substrate. As the indium concentration rises, the (002) diffraction peak intensity decreases and full width at half-maximum of (002) diffraction peak broaden resulting from degradation of crystallinity. Fig. 4 (a) shows a magnified GIXRD patterns of (002) peak. It is observed that the Braggs angle shift to lower angles with increasing indium doping concentrations. It is noted that the ionic radius of In (0.81 Å) is larger than Zn (0.74 Å) [11]. Based on the Bragg's law, the Bragg angle shifts to lower angles, due to the larger lattice constant induced by In incorporation. The crystallite size along (002) direction is estimated according to $t = 0.9\lambda/B\cos\theta$, where λ is the x-ray wavelength and θ is the Bragg diffraction angle [12]. Fig. 4 (b) shows that the un-doped films have larger crystallite size than the doped films, and the crystallite size tends to decrease as doping concentration increases. This may be due to the fact that indium prevents the orderly arrangement and increases number of nucleation centers. Fig. 5 shows the resistivity (ρ), carrier concentration (n), and Hall mobility (μ) of different In/(Zn + In) atomic ratios. The minimum resistivity of $1.8\times10^{-3}\,\Omega$ cm was achieved at approximately 8 at.% indium doping. Both the carrier concentration and Hall mobility

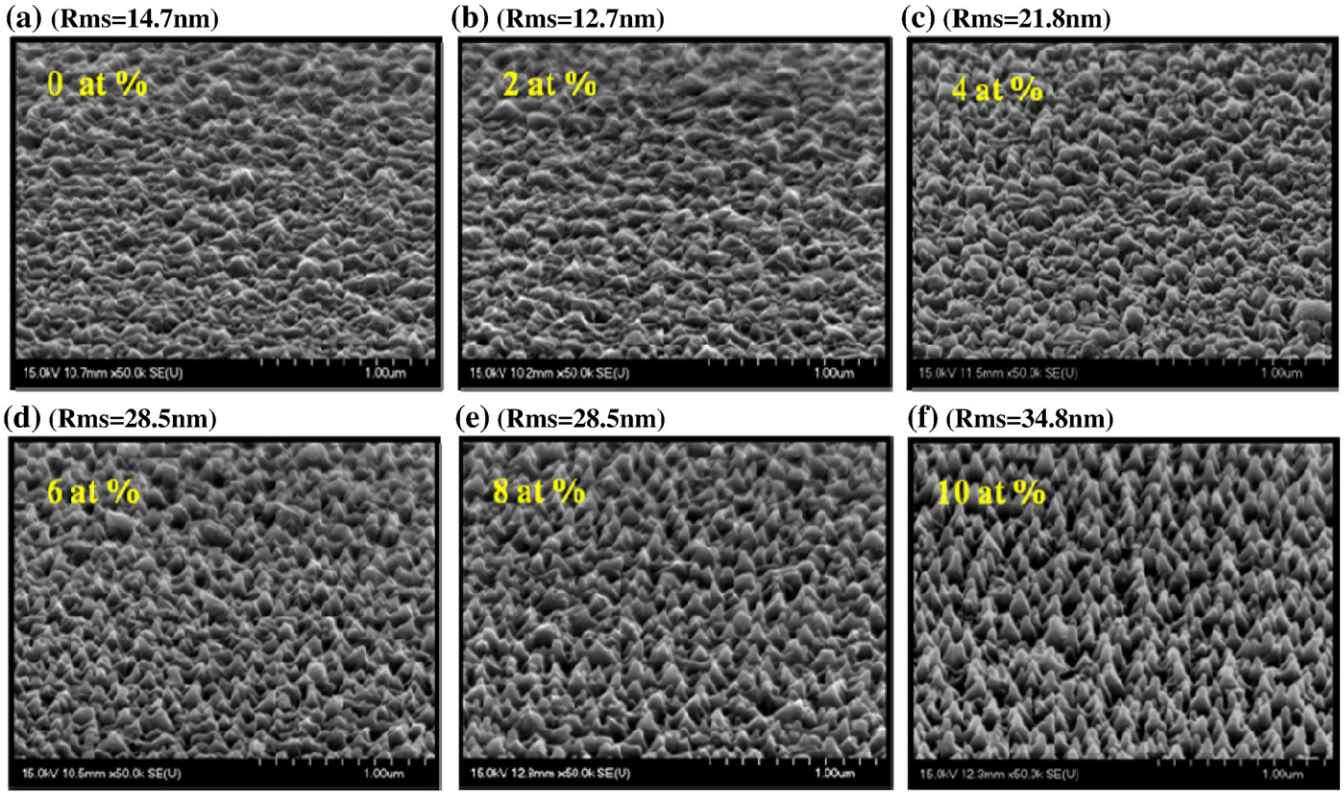

Fig. 2. SEM images (tilt angle) of different indium doping concentration from 0 at.% to 10 at.% (a) 0 at.% (Rms = 14.7 nm)(b) 2 at.% (Rms = 12.7 nm) (c) 4 at.% (Rms = 21.8 nm) (d) 6 at.% (Rms = 28.5 nm) (e) 8 at.% (Rms = 28.5 nm) (f) 10 at.% (Rms = 34.8 nm).

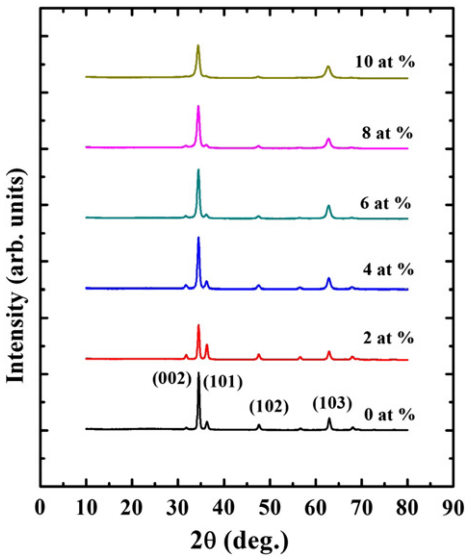

Fig. 3. GIXRD patterns of different indium-doped ZnO films deposited by APPJ at substrate temperature of 200 °C.

initially increase with indium doping concentrations; however, the carrier concentration gradually decreases beyond 8 at.%. When the doping concentration is low, indium atoms effectively occupy the

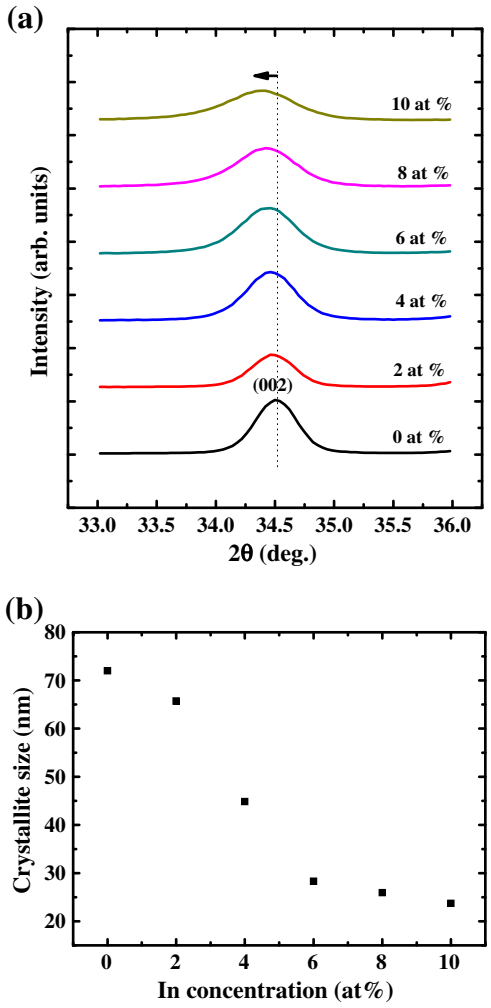

Fig. 4. (a) The magnified GIXRD patterns of (002) peak (b) crystalline size estimated along (002) peak with different indium doping concentration.

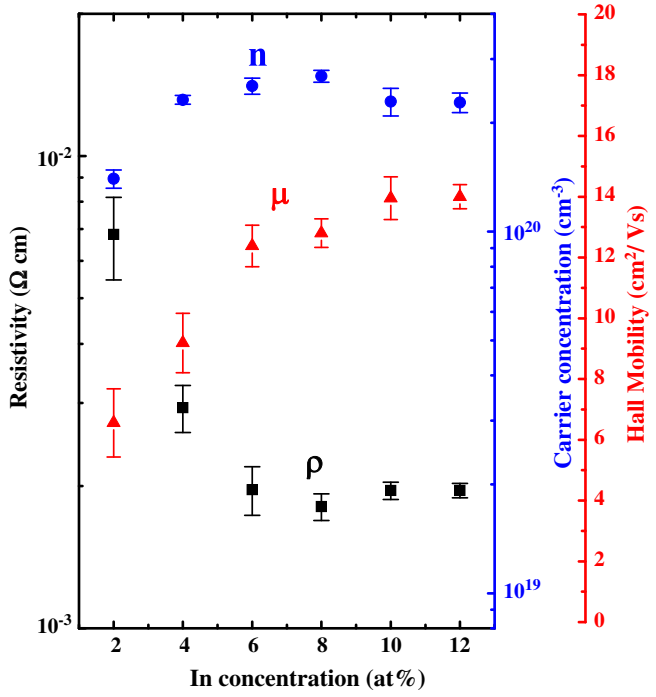

Fig. 5. Shows the resistivity (ρ), carrier concentration (n), and Hall mobility (μ) of different In/(Zn + In) atomic ratios.

substitutional sites to generate free electrons resulting in the rise of carrier concentration. While the doping concentration is higher than 8 at.%, the poor crystallinity may be responsible for the degraded carrier concentration. The structural defects can trap donors and free carriers result in the decrease of carrier concentration [13,14]. Also, the clustering or segregation of dopants may decrease the carrier concentration of TCO films with excess dopants [15,16]. Fig. 6 depicts transmission spectrum of ZnO films with different indium concentrations. The inserted graph shows the magnified absorption band edge. All films exhibited that average transmittance in visible region is more than 80%. The absorption edge shows a shift towards shorter wavelength from 0 at.% to 8 at.%. It has been reported that the increase in the optical band gap with an increase in carrier concentration. This phenomenon is known as Burnstein–Moss effect [17]. The optical bandgap is estimated by extrapolating the square of absorption coefficient versus the photon energy curve [18]. The

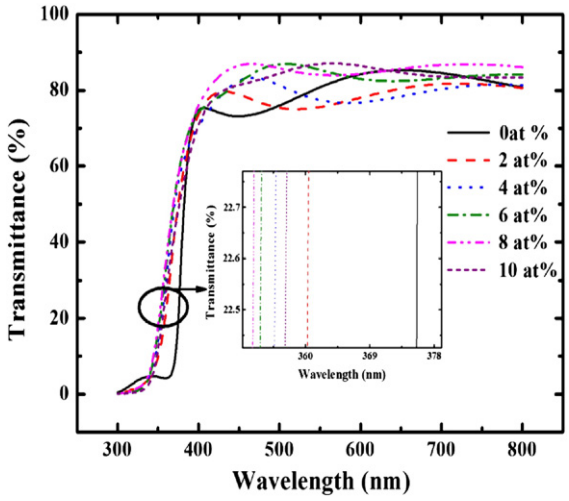

Fig. 6. Transmission spectrum of IZO films with different indium doping concentration.

Table 1
Optical bandgap of different indium doping concentration.

	0 at.%	2 at.%	4 at.%	6 at.%	8 at.%	10 at.%	12 at.%
Optical bandgap (eV)	3.28	3.41	3.49	3.51	3.51	3.51	3.47

bandgap values of different indium doping are listed in Table 1. The optical bandgap initially tends to rise with indium doping concentration. It is seen that the optical bandgap nearly saturates around 6 at.% to 10 at.%. Beyond 10%, a decline of bandgap is observed at 12 at.%.

4. Conclusion

In summary, we have demonstrated that indium-doped ZnO films deposited on glass utilizing atmospheric pressure plasma jet. This technique is a simple and inexpensive method. The thin films are polycrystalline with a preferred orientation along (002) plane and grain size tend to decrease as doping concentration increases. The SEM shows that the surface morphology is affected by indium doping. The films show needlelike geometry from 6 at.% to 10 at.% resulting in the rougher surface. The films prepared with 8 at.% indium-doped zinc oxide show a low resistivity of $1.8\times10^{-3}\,\Omega\,\mathrm{cm}$, a carrier concentration of $2.69\times10^{20}\,\mathrm{cm}^{-3}$, a mobility of $12.86\,\mathrm{cm}^2/\mathrm{V\text{-}s}$, a band gap of 3.51 eV and a transmittance of about 80% in the visible range.

References

[1] M.H. Han, J.H. Noh, T.I. Lee, J.H. Choi, K.W. Park, H.S. Hwang, K.M. Song, H.K. Baik, Plasma Process. Polym. 5 (9) (2008) 861.
[2] H.-K. Ha, M. Yoshimoto, H. Koinuma, B.-K. Moon, H. Ishiwara, Appl. Phys. Lett. 68 (21) (1996) 2965.
[3] K. Maruyama, I. Tsumagari, M. Kanezawa, Y. Gunji, M. Morita, M. Kogoma, S. Okazaki, J. Mater. Sci. Lett. 20 (5) (2001) 481.
[4] K. Ramamoorthy, K. Kumar, R. Chandramohan, K. Sankaranarayanan, R. Saravanan, I.V. Kityk, P. Ramasamy, Opt. Commun. 262 (1) (2006) 91.
[5] V. Bhosle, A. Tiwari, J. Narayan, J. Appl. Phys. 100 (3) (2006) 033713.
[6] T. Yamada, A. Miyake, S. Kishimoto, H. Makino, N. Yamamoto, T. Yamamoto, Appl. Phys. Lett. 91 (5) (2007) 051915.
[7] D.H. Kim, N.G. Cho, H.G. Kim, W.-Y. Choi, J. Electrochem. Soc. 154 (11) (2007) H939.
[8] I. Volintiru, M. Creatore, B.J. Kniknie, C.I.M.A. Spee, M.C.M.v.d. Sanden, J. Appl. Phys. 102 (4) (2007) 043709.
[9] O.V. Penkov, H.-J. Lee, V.Y. Plaksin, R. Mansur, J.H. Kim, Thin Solid Films 518 (22) (2010) 6160.
[10] Y. Suzaki, S. Ejima, T. Shikama, S. Azuma, O. Tanaka, T. Kajitani, H. Koinuma, Thin Solid Films 506–507 (2006) 155.
[11] M.P. Taylor, D.W. Readey, M.F.A.M.v. Hest, C.W. Teplin, J.L. Alleman, M.S. Dabney, L.M. Gedvilas, B.M. Keyes, B. To, J.D. Perkins, D.S. Ginley, Adv. Funct. Mater. 18 (20) (2008) 3169.
[12] A. Mondal, N. Mukherjee, S. Kumar Bhar, D. Banerjee, Thin Solid Films 515 (4) (2006) 1255.
[13] N. Taga, Y. Shigesato, M. Kamei, The 46th International Symposium of the American Vacuum Society, AVS, Seattle, Washington (USA), 2000, 1663 pp.
[14] P.K. Song, Y. Shigesato, M. Kamei, I. Yasui, Jpn. J. Appl. Phys. 38 (1999) 2921–2927.
[15] D.-J. Lee, H.-M. Kim, J.-Y. Kwon, H. Choi, S.-H. Kim, K.-B. Kim, Adv. Funct. Mater. (2010) 1.
[16] K.H. Kim, K.C. Park, D.Y. Ma, J. Appl. Phys. 81 (12) (1997) 7764.
[17] I. Hamberg, C.G. Granqvist, K.F. Berggren, B.E. Sernelius, L. Engström, Phys. Rev. B 30 (6) (1984) 3240.
[18] G.A. Hirata, J. McKittrick, J. Siqueiros, O.A. Lopez, T. Cheeks, O. Contreras, J.Y. Yi, J. Vacuum Sci. Technol. A Vacuum Surf. Films 14 (3) (1996) 791.